

# Fluorescence Anisotropy Spectra Disclose the Role of Disorder in Optical Spectra of Branched Intramolecular-Charge-Transfer Molecules

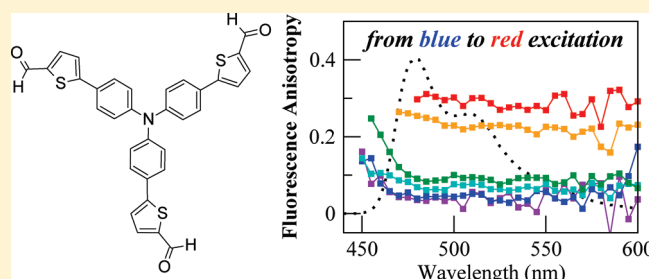
Cristina Sissa,<sup>†</sup> Anna Painelli,<sup>†</sup> Mireille Blanchard-Desce,<sup>‡</sup> and Francesca Terenziani<sup>\*,†</sup>

<sup>†</sup>Dipartimento di Chimica GIAF and INSTM-UdR Parma, Università di Parma, Parco Area delle Scienze 17/a, 43124 Parma, Italy

<sup>‡</sup>Chimie et Photonique Moléculaires (CNRS, UMR 6510), Université de Rennes 1, 35042 Rennes, France

**S** Supporting Information

**ABSTRACT:** Fluorescence excitation and emission spectra and corresponding anisotropies of branched intramolecular charge-transfer (ICT) chromophores are reported. To unravel the role of disorder related to polar solvation, we collected spectra of molecules with octupolar ( $C_3$ ) symmetry in glasses obtained from solvents of different polarity. Thermal disorder related to polar solvation is demonstrated by the dependence of fluorescence excitation/emission spectra and anisotropy spectra on the emission/excitation wavelength. In particular, for excitation in the red edge of the absorption band, the fluorescence anisotropy signal deviates from the 0.1 value expected for octupolar chromophores, approaching the limiting 0.4 value. A qualitatively different result is observed in nonpolar solvents. Based on essential-state models for ICT chromophores, we develop an original approach for the calculation of anisotropy spectra that quantitatively reproduces experimental data. The model, accounting for the coupling between electrons and molecular vibrations and polar solvation, leads to a thorough understanding of the phenomena at the basis of solute–solvent interactions in branched ICT chromophores. A clear distinction is made between symmetry-breaking phenomena in the excited state and disorder-induced lowering of the molecular symmetry. Their relation with red-edge effects is pointed out.



## 1. INTRODUCTION

Organic molecules with intramolecular charge-transfer (ICT) properties are widely studied in view of their potential applications in the fields of polarity sensing,<sup>1–4</sup> organic electronics,<sup>5–8</sup> photovoltaics,<sup>9–16</sup> and nonlinear optics,<sup>17–24</sup> to name a few. ICT molecules are typically characterized by the presence of one or more electron-donor (D) and electron-acceptor (A) groups, connected by  $\pi$ -conjugated structures. The simplest case is represented by so-called push–pull chromophores, but more extended, branched structures with multiple D and A groups have recently attracted attention for their enhanced nonlinear optical responses<sup>17–24</sup> and light-harvesting capabilities.<sup>10,25–27</sup> Branched ICT molecules comprise quadrupolar structures (with an A– $\pi$ –D– $\pi$ –A or D– $\pi$ –A– $\pi$ –D motif), octupolar molecules [with an A( $-\pi$ –D)<sub>3</sub> or D( $-\pi$ –A)<sub>3</sub> motif], and more involved dendritic structures of different size and generation.

To exploit branched ICT molecules for specific tasks, a good understanding of their excited states is needed. In fact, depending on the strength of the coupling among the different molecular branches, either localized or delocalized excited states can be expected, with important consequences for the material properties and behavior.<sup>28</sup> On the other hand, the nature itself of molecular excited states is strongly affected by the molecular environment.

In this article, we investigate the optical spectra of a couple of representative octupolar ICT molecules, **O1** and **O2**, and of the

push–pull molecule **D1**, which mimics the molecular branch of **O1** (Scheme 1). A thorough analysis of the spectra collected in environments of different polarities leads to a fine understanding of the nature of the excited states of octupolar dyes and of the subtle effects of disorder induced by polar solvation in multi-branched ICT chromophores. The detailed modeling, based on essential-state approaches, of fluorescence anisotropy spectra collected in glassy solvents unravels the role of thermal disorder (inhomogeneous broadening) in polar matrixes, clarifying the physical origin of some peculiar phenomena commonly referred to as “red-edge effects” and recognizing the role of disorder-induced symmetry lowering.

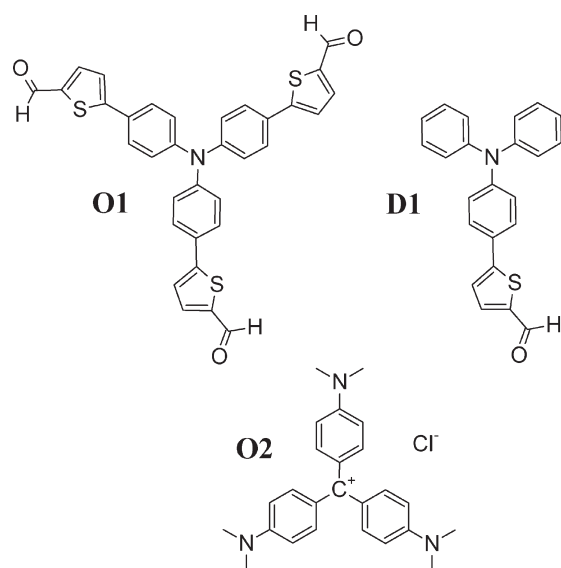
## 2. EXPERIMENTAL SECTION

**2.1. Materials.** Compounds **O1** and **D1** were synthesized as previously reported.<sup>29</sup> **O2** (known as Crystal Violet) was purchased from Sigma (ACS reagent, 91.7%). The solvents used were 2-methyltetrahydrofuran (2-MeTHF, Sigma-Aldrich, anhydrous, >99.0%), 1,2-propanediol (or propylene glycol, PG, Sigma-Aldrich, puriss., >99.5%), and decahydronaphthalene

**Received:** March 23, 2011

**Revised:** April 15, 2011

**Published:** May 10, 2011

**Scheme 1. Molecular Structures and Naming of the Investigated Compounds**

(DHN, also called decalin, Sigma-Aldrich, *cis* + *trans* mixture, anhydrous,  $\geq 99.0\%$ ). 2-MeTHF was used after overnight storage on molecular sieves (0.3 nm). Other solvents were used as received. Compound **O2** was studied only in PG solutions, because it is not soluble in DHN and it undergoes aggregation in 2-MeTHF.

**2.2. Fluorescence and Fluorescence Anisotropy Measurements.** Fluorescence and fluorescence anisotropy (emission and excitation) spectra were recorded on a Fluoromax-3 Horiba Jobin-Yvon spectrofluorometer equipped with a xenon lamp as the excitation source and excitation and emission Glan–Thompson automatic polarizers for anisotropy measurements (single-channel L format). Fluorescence anisotropy is defined as<sup>30</sup>

$$r = \frac{I_{\parallel} - I_{\perp}}{I_{\parallel} + 2I_{\perp}} \quad (1)$$

where  $I_{\parallel}$  and  $I_{\perp}$  are the emission intensities when the emission polarizer is oriented parallel or perpendicular to the excitation polarizer, respectively. Experimentally, anisotropy is obtained as<sup>30</sup>

$$r = \frac{I_{VV} - GI_{VH}}{I_{VV} + 2GI_{VH}} \quad (2)$$

where the two subscripts indicate the orientation of the excitation and emission polarizers, respectively. For example,  $I_{VV}$  and  $I_{VH}$  are the fluorescence intensities measured for vertically polarized excitation (first subscript) and vertically and horizontally polarized emission (second subscript), respectively. The  $G$  factor measures the ratio of the sensitivities of the detection system for vertically and horizontally polarized light and is determined using horizontally polarized excitation:  $G = I_{HV}/I_{HH}$ . The  $G$  factor is independent of the excitation wavelength, so that a single value can be used for determining fluorescence excitation anisotropy spectra; it varies instead according to the emission wavelength ( $\lambda_{em}$ ), so that the  $G(\lambda_{em})$  dependence has to be measured to obtain fluorescence emission anisotropy spectra.

Spectra were measured after the solutions had been cooled with an Oxford Instruments OptistatDN cryostat providing a

controlled low-temperature exchange gas environment for the sample contained in quartz cuvettes specially designed for cryogenics (supplied by the FAVS Company, Bologna, Italy). 2-MeTHF solutions, PG solutions, and DHN solutions were rapidly cooled (about 20 K per minute) to 77, 190, and 210 K, respectively, to obtain transparent glasses (or supercooled highly viscous liquids). Under these conditions, the motion of solute molecules during the excited-state lifetime can be safely neglected. Specifically, for the dipolar chromophore **D1**, we measured anisotropy values exceeding 0.3 (i.e., approaching the limiting 0.4 value for random distributions); this gives confirmation that depolarization effects due to orientational motions during the excited-state lifetime are indeed negligible.<sup>30</sup>

### 3. THEORETICAL APPROACH

**3.1. Essential-State Models for Dipolar and Octupolar ICT Molecules.** The low-energy spectroscopic behavior of ICT molecules is governed by a few effective states. In recent years, essential-state models have been developed for the description of ICT molecules of different complexity and symmetry, including dipolar,<sup>31,32</sup> quadrupolar<sup>33,34</sup> and octupolar chromophores.<sup>35,36</sup> The charge-resonance model for dipolar (push–pull) chromophores is based on two basis states,<sup>37,38</sup> corresponding to the two resonant forms, the neutral,  $N$ , and the zwitterionic,  $Z$ , structures. The two basis states are separated by an energy gap,  $2\eta$ , and mixed by the charge-resonance integral,  $-\sqrt{2}t$ . The ground and excited states,  $|g\rangle = \sqrt{1-\rho}|N\rangle + \sqrt{\rho}|Z\rangle$  and  $|e\rangle = \sqrt{\rho}|N\rangle - \sqrt{1-\rho}|Z\rangle$ , respectively, are defined by a single parameter,  $\rho$ , describing the degree of charge transfer in the ground state ( $0 \leq \rho \leq 1$ ). The zwitterionic state has a large dipole moment,  $\mu_0$ , and all other matrix elements of the dipole moment operator are disregarded.<sup>37</sup> The excitation energy and the permanent and transition dipole moments can be expressed as functions of  $\rho$  (see the Supporting Information).

Octupolar chromophores,  $D(-\pi-A)_3$  or  $A(-\pi-D)_3$ , with planar structures are characterized by  $D_{3h}$  symmetry. In an essential-state description, they can be described as resonating between four basis states.<sup>35,39</sup> For noncharged molecules (such as **O1**), one can identify a neutral form,  $|N\rangle$ , and three charge-separated states,  $|Z_1\rangle$ ,  $|Z_2\rangle$ , and  $|Z_3\rangle$ , corresponding to the three degenerate states where a charge is transferred from the central core to each one of the three branches (or backward). The octupolar molecule **O2** instead bears a net positive charge. The standard model for octupolar chromophores is easily generalized to this specific case: the resonant structure where the central carbon atom bears the positive charge corresponds to the  $|N\rangle$  state of neutral octupolar chromophores and the three degenerate states obtained by displacing the positive charge along each one of the three molecular branches correspond to the zwitterionic states  $|Z_1\rangle$ ,  $|Z_2\rangle$ , and  $|Z_3\rangle$  of neutral octupolar dyes.<sup>36</sup> In principle, the dipole moment of charged species is ill-defined; however, if one expands the charge distribution in terms of monopolar and dipolar charges located at the molecular center, one can see that the monopole charge is invariant in all basis states, so that it becomes irrelevant in the subsequent discussion, and the model precisely maps onto the standard model for neutral chromophores.<sup>36</sup> In all cases, we define  $2\eta$  as the energy gap between the three degenerate  $|Z_i\rangle$  states and the  $|N\rangle$  state, while  $-\sqrt{2}t$  is the matrix element that mixes  $|N\rangle$  to each one of the three  $|Z_i\rangle$  states. The three arms of the molecule are interchanged by a  $C_3$  symmetry axis: the three degenerate

basis states are then conveniently combined into a totally symmetric wave function,  $|Z_+\rangle = (|Z_1\rangle + |Z_2\rangle + |Z_3\rangle)/\sqrt{3}$ , and two degenerate  $E$ -symmetry functions that can be chosen as  $|c_1\rangle = (2|Z_1\rangle - |Z_2\rangle - |Z_3\rangle)/\sqrt{6}$  and  $|c_2\rangle = (|Z_2\rangle - |Z_3\rangle)/\sqrt{2}$ , or as any (orthogonal) linear combination thereof. The wave function  $|N\rangle$  has the same symmetry as  $|Z_+\rangle$ : the two states are mixed to give two totally symmetric states, the ground state  $|g\rangle = \sqrt{1-\rho}|N\rangle + \sqrt{\rho}|Z_+\rangle$  and an excited state  $|e\rangle = \sqrt{\rho}|N\rangle - \sqrt{1-\rho}|Z_+\rangle$ , with  $\rho$  measuring the amount of charge transferred in the ground state from the central group toward the three lateral branches, proportional to the molecular octupolar moment. The two degenerate  $E$ -symmetry states,  $c_1$  and  $c_2$ , stay unmixed and are accessible by linear absorption. The  $e$  state is dark (not accessible by linear absorption), but can be reached by two-photon absorption. The three degenerate  $|Z_i\rangle$  states have dipole moments of equal length,  $\mu_0$ , pointing along the three molecular arms. Expressions for transition energies and corresponding dipole moments are reported in the Supporting Information.

The electronic models for dipolar and octupolar chromophores have been extended to account for the coupling between electronic and vibrational degrees of freedom and for polar solvation. The resulting models have proven fairly successful in the description of linear and nonlinear optical spectra of several chromophores.<sup>29,32–36</sup> For dipolar chromophores, the minimal model accounts for one effective molecular vibration.<sup>32</sup> For octupolar chromophores, at least one degree of freedom for each molecular arm must be accounted for: the corresponding three vibrational coordinates combine to give a symmetric coordinate and two degenerate  $E$ -symmetry modes. For either dipolar or octupolar chromophores, each basis state is assigned a harmonic potential energy surface (PES) with the same frequency,  $\omega_v$ , but with displaced minima along the relevant vibrational coordinate(s), to describe the different equilibrium geometry associated with each state. The strength of the coupling is conveniently measured by  $\varepsilon_{sp}$ , the vibrational relaxation energy associated with the  $|N\rangle \rightarrow |Z_i\rangle$  process.<sup>35</sup>

The Hamiltonian that describes the coupled electronic and vibrational problem is solved nonadiabatically. The relevant basis is obtained as the direct product of the electronic basis states times the eigenstates of the harmonic oscillators associated with the effective molecular coordinates. The eigenstates of each harmonic oscillator define an infinite basis set; therefore, we truncated the basis disregarding states with a total number of vibrational quanta (summing on all oscillators) larger than  $M$ . The truncated basis increases as  $2M$  for dipoles and as  $2\sum_{m=0}^{M-1}(m+2)(m+1)$  for octupoles. The relevant Hamiltonian matrix can be diagonalized for finite  $M$  to get numerically exact nonadiabatic eigenstates. The minimum  $M$  required to achieve convergence depends on the model parameters and the properties of interest. The results presented here were obtained with  $M = 10$  for **D1** and **O1** and with  $M = 8$  for **O2**, and they were checked for convergence.

Polar solvation can be taken into account by describing the solvent as a continuum dielectric medium. The polar solvent molecules reorient around the solute to generate a reaction field,  $F_{or}$ . For dipolar chromophores, the reaction field is oriented along the molecular axis ( $x$ ), so that  $F_{or} = F_x$ . For octupolar structures, we assume a planar geometry, so that only the two components of the reaction field in the molecular  $xy$  plane,  $F_x$  and  $F_y$ , are relevant. The reaction field enters the molecular Hamiltonian through the term  $-\hat{\mu}_x F_x - \hat{\mu}_y F_y$ , where  $\hat{\mu}_x$  and  $\hat{\mu}_y$  are the two components of the molecular dipole moment operator (only  $\hat{\mu}_x$  has to be considered for dipolar molecules). The elastic restoring force for the solvent is  $\mu_0^2 F_{or}^2 / (4\varepsilon_{or})$ , where

$F_{or}^2 = F_x^2 + F_y^2$ , and  $\varepsilon_{or}$ , the solvation relaxation energy, increases with solvent polarity.<sup>31</sup> These expressions ensure that the equilibrium value of the reaction field is proportional to the solute dipole moment. At finite temperatures, thermal disorder is responsible for fluctuations of the reaction field around the equilibrium value, leading to a distribution of  $F_{or}$  values, according to the Boltzmann probability.<sup>32,35</sup> The polar component of the reaction field, associated with the orientational motion of the solvent molecules, describes a slow motion with respect to both electronic and vibrational degrees of freedom. As a consequence,  $F_x$  and  $F_y$  can be treated as classical variables. Therefore, we define a grid of  $F_{or}$  values (a two-dimensional grid in the  $F_x F_y$  plane for octupolar chromophores and a one-dimensional array on the  $F_x$  line for dipolar molecules), and for each point of the grid, we diagonalize the nonadiabatic  $F_{or}$ -dependent molecular Hamiltonian to get  $F_{or}$ -dependent eigenstates.

For each point of the grid, absorption spectra are calculated by assigning each transition a Gaussian line shape with fixed standard deviation  $\sigma$

$$A(\tilde{\nu}) = \sum_i A_i(\tilde{\nu}) \propto \sum_i \frac{\tilde{\nu} \mu_{gi}^2}{\sigma \sqrt{2\pi}} \exp \left[ -\frac{1}{2} \left( \tilde{\nu} - \frac{\tilde{\nu}_{ig}}{\sigma} \right)^2 \right] \quad (3)$$

where  $i$  runs over excited nonadiabatic eigenstates,  $\mu_{gi}$  is the dipole moment for the transition from the ground state ( $g$ ) to the  $i$ th state, and  $\tilde{\nu}_{ig}$  is the wavenumber associated with the  $g \rightarrow i$  transition. Similarly, fluorescence spectra are calculated for each point of the  $F_{or}$  grid, taking into account the transitions from the emissive state toward lower-energy states and assigning each transition a Gaussian line shape with fixed standard deviation  $\sigma$

$$F(\tilde{\nu}) = \sum_i F_i(\tilde{\nu}) \propto \sum_i \frac{\tilde{\nu}^3 \mu_{fi}^2}{\sigma \sqrt{2\pi}} \exp \left[ -\frac{1}{2} \left( \tilde{\nu} - \frac{\tilde{\nu}_{fi}}{\sigma} \right)^2 \right] \quad (4)$$

where  $i$  runs over nonadiabatic eigenstates,  $\mu_{fi}$  is the dipole moment for the transition from the emissive excited state ( $f$ ) to the  $i$ th state, and  $\tilde{\nu}_{fi}$  is the wavenumber associated with the  $f \rightarrow i$  transition. The definition of the emissive state is tricky in the nonadiabatic picture, because the eigenstates cannot be classified as belonging to the ground-state or excited-state manifold. Because the lowest-energy electronic excitation is optically allowed for both dipolar and octupolar molecules, we identify the emissive state as the first nonadiabatic excited state with a sizable transition dipole moment from the ground state (i.e., having the character of an “electronically excited state”).

Total absorption and fluorescence spectra are finally obtained as an incoherent sum of the spectra obtained for each value of the reaction field, each spectrum being weighted according to the relevant Boltzmann probability. Accordingly, the proposed model for polar solvation not only accounts for the modulation of the energy of molecular states in polar solvents (i.e., for solvatochromism) as well as their temperature dependence, but also describes inhomogeneous broadening phenomena associated with polar solvation. At any temperature, in liquid solutions, the Boltzmann distribution relevant to the absorption process is based on the energy of the ground state, whereas that relevant to the fluorescence process is based on the energy of the emissive state. Care must be taken, however, when dealing with frozen solutions: in that case, the solvent cannot relax after the solute excitation (orientational motions are hindered by the glassy or extremely viscous matrix), and the same Boltzmann



distribution based on the ground-state energy applies to the calculation of both absorption and fluorescence spectra.

**3.2. Calculation of Fluorescence Anisotropy Spectra.** The calculation of fluorescence anisotropy spectra is not trivial, and two subtle phenomena must be carefully considered. First, one has to recognize that working with glassy matrixes has major consequences in the presence of inhomogeneous broadening. In a frozen inhomogeneous distribution of solute molecules, in fact, monochromatic light preferentially excites a subset of molecules from the inhomogeneous distribution (those absorbing at that specific wavelength). This phenomenon is called energy photoselection.<sup>40</sup> Because the matrix is rigid, the relaxation along the solvation coordinate is hindered, and only vibrational relaxation takes place before fluorescence emission. Therefore, the emission spectrum is that relevant to the specific subset of photoselected molecules, with a relaxed geometry along the internal coordinates but in the frozen solvent configuration. Analogously, when calculating fluorescence excitation and excitation anisotropy spectra, one must consider energy photoselection in emission: the emission detected at the selected wavelength has a dominant contribution from the specific subset of excited molecules, from the inhomogeneous distribution, emitting at that specific wavelength. The second important aspect concerns polarization photoselection:<sup>30</sup> when excited with a polarized light beam, molecules with the absorption transition dipole moment oriented along the direction of polarization are preferentially excited. Moreover, because anisotropy is measured in solutions of randomly oriented molecules, an appropriate averaging over all possible orientations has to be performed.

In our calculations, inhomogeneous broadening is associated with a distribution of reaction fields weighted according to the Boltzmann distribution for the ground-state energy (frozen solutions). For the calculation of fluorescence emission and emission anisotropy spectra, we account for energy photoselection by considering the probability, for each point of the  $F_{\text{or}}$  grid, that the incident photons at the excitation wavelength are absorbed by the corresponding subset of solute molecules. For fluorescence excitation and excitation anisotropy spectra, we consider the probability, for each point of the  $F_{\text{or}}$  grid, that photons at the detection wavelength are emitted by the corresponding subset of solute molecules. Concerning the problem of orientational photoselection, ref 41 suggests a very efficient way to calculate the fluorescence intensity for polarized excitation beams when the sample is randomly oriented in a rigid matrix. The following expressions allow estimation of the fluorescence intensity for parallel ( $I_{\parallel}$ ) and perpendicular ( $I_{\perp}$ ) polarizers

$$\begin{aligned} I_{\parallel} &\propto \frac{|\vec{\mu}_{\text{em}}|^2 \cdot |\vec{\mu}_{\text{abs}}|^2 + 2(\vec{\mu}_{\text{em}} \cdot \vec{\mu}_{\text{abs}})^2}{15} \\ I_{\perp} &\propto \frac{2|\vec{\mu}_{\text{em}}|^2 \cdot |\vec{\mu}_{\text{abs}}|^2 - (\vec{\mu}_{\text{em}} \cdot \vec{\mu}_{\text{abs}})^2}{15} \end{aligned} \quad (5)$$

where  $\vec{\mu}_{\text{abs}}$  and  $\vec{\mu}_{\text{em}}$  are the transition dipole moment vectors relevant to the absorption and emission processes, respectively.

The expressions in eq 5 can be generalized to account for the presence of several (nonadiabatic) excited states and the wavelength dependence of absorption and emission intensities as follows

$$\begin{aligned} I_{\parallel}(\lambda_{\text{exc}}, \lambda_{\text{em}}) &= \frac{1}{15} \sum_{i,j} A_i(\lambda_{\text{exc}}) F_j(\lambda_{\text{em}}) (1 + 2 \cos^2 \theta_{ij}) \\ I_{\perp}(\lambda_{\text{exc}}, \lambda_{\text{em}}) &= \frac{1}{15} \sum_{i,j} A_i(\lambda_{\text{exc}}) F_j(\lambda_{\text{em}}) (2 - \cos^2 \theta_{ij}) \end{aligned} \quad (6)$$

where  $A_i(\lambda_{\text{exc}})$  measures the absorbance from the ground state toward the  $i$ th nonadiabatic excited state ( $i$  runs over all nonadiabatic excited states), at the excitation wavelength,  $\lambda_{\text{exc}}$ ;  $F_j(\lambda_{\text{em}})$  is the fluorescence intensity from the emitting state toward the  $j$ th state ( $j$  runs over all nonadiabatic states with lower energy than the emitting state) at the wavelength  $\lambda_{\text{em}}$ ;  $\theta_{ij}$  is the angle formed between the absorption transition dipole moment from the ground state to the  $i$ th state and the fluorescence transition dipole moment from the emitting state to the  $j$ th state. In the calculation of emission anisotropy spectra, the excitation wavelength ( $\lambda_{\text{exc}}$ ) is kept fixed as  $\lambda_{\text{em}}$  is varied. In this case, the absorbance term,  $A_i(\lambda_{\text{exc}})$ , accounts for energy photoselection: each excited state  $i$  contributes to the polarized spectrum according to its absorbance at the excitation wavelength. In the calculation of fluorescence excitation anisotropy, the emission wavelength is fixed as the excitation wavelength is varied, and  $F_j(\lambda_{\text{em}})$  accounts for energy photoselection: each state  $j$  contributes to the polarized spectrum according to the emissivity of the emitting state toward the  $j$ th state at the emission wavelength.

To take into account the effects related to inhomogeneous broadening, the two polarized emission intensity terms,  $I_{\parallel}$  and  $I_{\perp}$ , have to be weighted separately for the relevant Boltzmann distribution. This is a key point: as  $I_{\parallel}$  and  $I_{\perp}$  are the results of two independent measurements, they must also be averaged over the inhomogeneous distribution as two independent quantities. Therefore,  $I_{\parallel}$  and  $I_{\perp}$  are calculated for each point of the  $F_{\text{or}}$  grid, and results are summed according to the (normalized) probability associated with each  $F_{\text{or}}$  value, giving the total polarized emission intensities,  $\bar{I}_{\parallel}$  and  $\bar{I}_{\perp}$ , that enter eq 1 to calculate the (emission or excitation) anisotropy.

## 4. RESULTS

Room-temperature absorption and fluorescence spectra of **D1** and **O1** dissolved in decahydronaphthalene (DHN), 2-methyltetrahydrofuran (2-MeTHF), and propylene glycol (PG) are reported in Figure 1. These solvents span a wide polarity range: DHN is a nonpolar solvent, 2-MeTHF has intermediate polarity, and PG is highly polar. This is confirmed by the solvatochromic behavior of the two chromophores, with the fluorescence band strongly red-shifted when going from DHN to 2-MeTHF to PG. The solvatochromic behaviors of **D1** and **O1** have recently been reported and discussed.<sup>29</sup> **D1** is a typical push–pull chromophore: the solvatochromism of its fluorescence band is naturally ascribed to the dipolar character of the excited state. **O1** has an octupolar character, and the solvatochromic behavior of its fluorescence is understood in terms of symmetry breaking (excitation localization) in the excited state.<sup>35</sup> Parameters of the essential-state models for **D1** and **O1** have been obtained through a careful analysis of their optical spectra.<sup>29</sup> The same molecular parameters allow the spectra in Figure 1 to be reproduced, fixing the solvent relaxation energies to  $\varepsilon_{\text{or}} = 0$ , 0.28, and 0.52 eV for DHN, 2-MeTHF, and PG, respectively.<sup>42</sup>

Figure 2 reports fluorescence excitation and emission spectra and corresponding anisotropy spectra of **D1** in glassy 2-MeTHF, collected after rapid cooling at 77 K. Excitation and emission spectra show typical features stemming from inhomogeneous broadening: the spectra shift to the red when the detection or excitation line is moved to the red. In fact, each chosen wavelength of emission or excitation preferentially selects a subset of molecules from the inhomogeneous distribution of the polar solvation coordinate ( $F_{\text{or}}$ ). Because this distribution is

frozen in the glassy matrix, the excitation or emission spectrum is obtained from the same subset of photoselected molecules. Anisotropy inside the excitation or emission band amounts to about 0.35, very close to the limiting value of 0.4 expected for

molecules having parallel absorption and emission transition dipole moments. This result provides confirmation of the good optical quality of the glassy matrix, excluding the matrix as a source of depolarization.

More interesting are the results obtained for the octupolar compound **O1**. Figure 3 reports fluorescence excitation and emission spectra and corresponding anisotropy spectra of **O1** in glassy 2-MeTHF, collected after rapid cooling at 77 K. The behavior of the excitation and emission spectra is similar to that observed for **D1** and is related to inhomogeneous broadening effects. Anisotropy spectra have instead a strikingly different behavior: excitation anisotropy increases inside the excitation band from a value lower than 0.1 on the blue side of the band to values exceeding 0.3 on the red side of the band, quite independently of the emission wavelength. Consistently with this result, emission anisotropy stays almost flat inside the emission band, with values going from about 0.1 to 0.3 when the excitation wavelength is moved from the blue to the red side of the absorption spectrum. Only in the narrow region of the Stokes shift (from 470 to 450 nm) is a sharp increase of the anisotropy observed.

The standard interpretation of anisotropy for planar molecules with 3-fold symmetry is based on the description of the molecule as constituted by three chromophores arranged on a plane according to a 3-fold symmetry axis.<sup>30,43,44</sup> In a polarization experiment, independently of the orientation of the absorption transition moment, after optical excitation, a redistribution of the excited-state energy among the three transition moments, through intramolecular transfer, leads to a fixed ratio of parallel and perpendicular intensity components. In the absence of extrinsic depolarization effects, the additivity law of polarization<sup>45</sup> gives the limiting polarization as  $p_0 = 1/7 = 0.143$  or, equivalently, the limiting anisotropy as  $r_0 = 0.1$ .<sup>30,43</sup>

The same result for the limiting anisotropy can be predicted in the framework of the four-level model for octupolar chromophores.

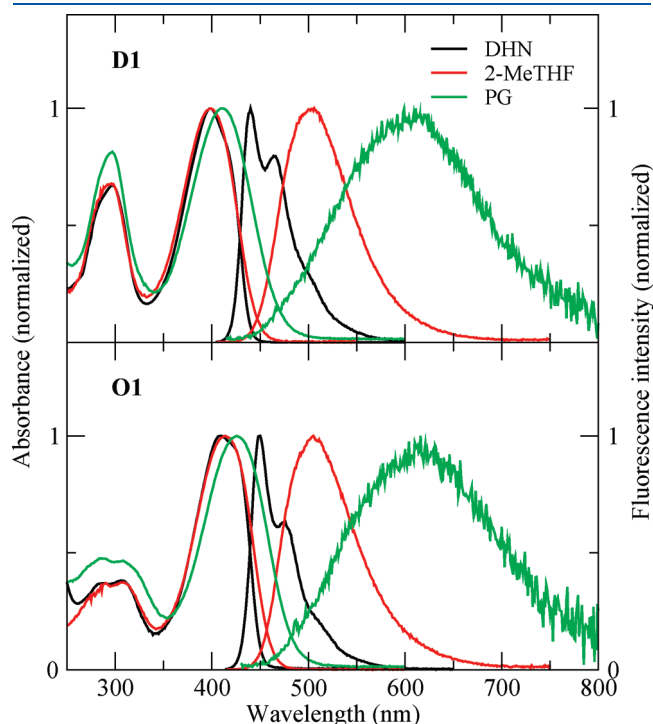


**Figure 1.** Room-temperature absorption and fluorescence spectra of (top) **D1** and (bottom) **O1** dissolved in decahydronaphthalene (DHN, black lines), 2-methyltetrahydrofuran (2-MeTHF, red lines), and propylene glycol (PG, green lines). For each sample, the excitation line for emission spectra was fixed at the wavelength of maximum absorption.

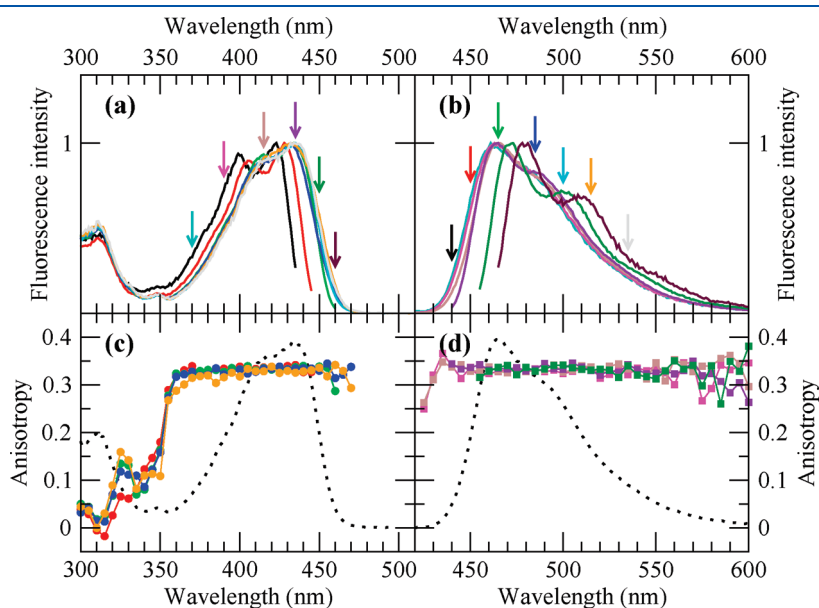


**Figure 2.** Spectra of **D1** in glassy 2-MeTHF at 77 K. (a) Fluorescence excitation spectra and (c) fluorescence excitation anisotropy spectra obtained by detecting at different emission wavelengths (440, 450, 465, 485, 500, 515, 535 nm), as indicated by the arrows of the corresponding colors in panel b. (b) Fluorescence emission spectra and (d) fluorescence emission anisotropy spectra obtained by exciting at different wavelengths (370, 390, 415, 435, 450, 460 nm), as indicated by the arrows of the corresponding colors in panel a. In panels c and d, dashed lines report representative excitation and emission spectra, respectively, as guides to the eyes.

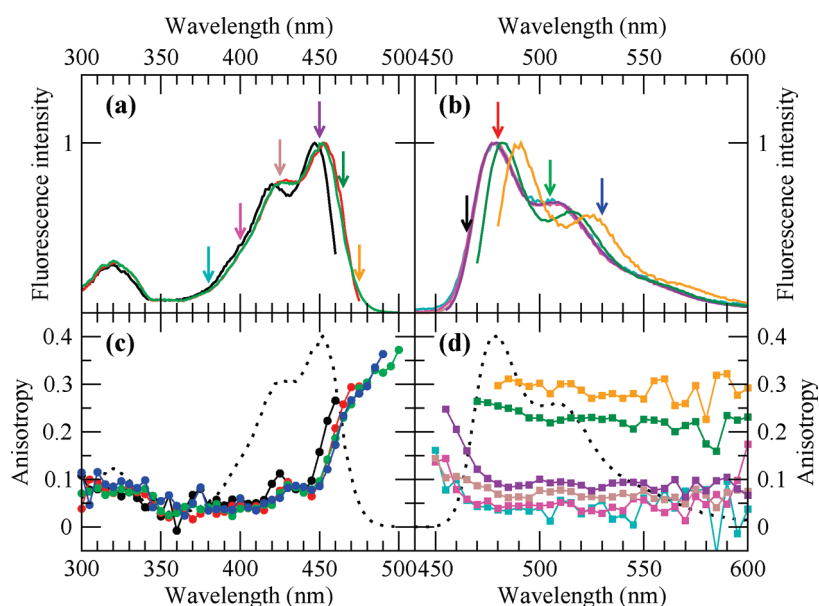
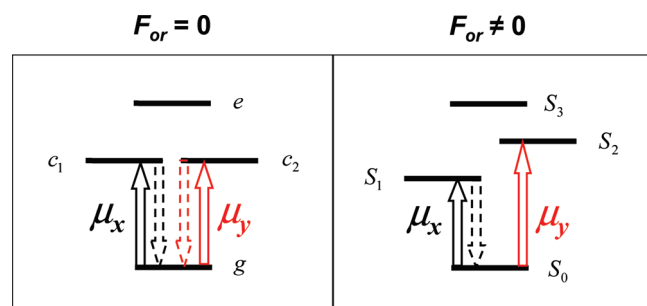


**Figure 3.** Spectra of **O1** in glassy 2-MeTHF at 77 K. (a) Fluorescence excitation spectra and (c) fluorescence excitation anisotropy spectra obtained by detecting at different emission wavelengths (465, 480, 505, 530 nm), as indicated by the arrows of the corresponding colors in panel b. (b) Fluorescence emission spectra and (d) fluorescence emission anisotropy spectra obtained by exciting at different wavelengths (380, 400, 425, 450, 465, 475 nm), as indicated by the arrows of the corresponding colors in panel a. In panels c and d, dashed lines report representative excitation and emission spectra, respectively, as guides to the eyes.

**Scheme 2. Energy Levels and Transition Dipole Moment Polarizations for an Octupolar Chromophore in the Essential-State Description: (Left) Symmetric System at  $F_{or} = 0$ , (Right) Symmetry-Lowered System as a Result of a Finite  $F_{or}$  Value**



The left panel of Scheme 2 shows the four essential energy levels for an octupolar chromophore. The two degenerate low-energy excited states, allowed by linear absorption, have transition dipole moments polarized along perpendicular directions.<sup>35</sup> Once the molecule has been excited along one particular polarization, the excitation can redistribute between the two degenerate excited states, so that emission occurs with equal probability from either one of the two degenerate excited states, with parallel or perpendicular polarization with respect to excitation. Again, the law of additivity of polarization leads to the limiting anisotropy of  $r_0 = 0.1$ .

Within our model, one can easily understand the effects of polar solvation. The ground state of octupolar chromophores has no permanent dipole moment, so that, at equilibrium,  $F_{or} = 0$ . However, at finite temperature, a distribution of reaction fields is expected, so that the molecules in solution can experience finite values of the reaction field.<sup>35</sup> In the presence of a finite  $F_{or}$ , the molecular symmetry is lowered, and the original states combine

to give new eigenstates, that we label  $S_0$  (ground state),  $S_1$ ,  $S_2$ , and  $S_3$ . In particular, the first two excited states, degenerate for  $F_{or} = 0$ , are split into the  $S_1$  and  $S_2$  states,<sup>36</sup> as depicted in the right panel of Scheme 2. In this case, according to the polarization of the excitation light, either the  $S_1$  or the  $S_2$  state will be populated, but emission, always occurring from the lowest-energy excited state, will invariably be polarized along one particular polarization ( $x$  in our scheme). This means that, when the red side of the absorption band (i.e., preferentially the  $S_1$  state) is excited, anisotropy will be high (near 0.4), whereas when the blue side of the absorption band (i.e., preferentially the  $S_2$  state) is excited, emission will be depolarized. The loss of symmetry of the molecules experiencing finite  $F_{or}$  values is the origin of the peculiar behavior of fluorescence anisotropy spectra observed for the octupolar compound **O1** and is therefore related to inhomogeneous broadening effects.

Essential-state models allow for a detailed calculation of fluorescence anisotropy spectra, based on the model parameters derived from the analysis of room-temperature spectra.<sup>29</sup> Calculated fluorescence excitation and emission spectra and corresponding anisotropy spectra of **O1** are reported in Figure 4. The spectra were calculated for a rigid matrix (no relaxation of the solvent distribution prior to fluorescence) at 90 K, the estimated glass transition temperature of 2-MeTHF.<sup>46</sup> The calculated spectra (Figure 4) reproduce remarkably well the experimental behavior (see Figure 3 for comparison), even if the Stokes shift is somewhat underestimated. The shapes of the excitation and emission spectra, as well as their shifts and/or changes in vibronic structure according to the emission or excitation wavelength, are in line with the experimental observations. However, the most remarkable result is given by the anisotropy spectra, which impressively match the experimental data in Figure 3.

In particular, the dependence of fluorescence anisotropy on the excitation wavelength is *quantitatively* reproduced (panel c), as is the dependence of anisotropy on the emission wavelength

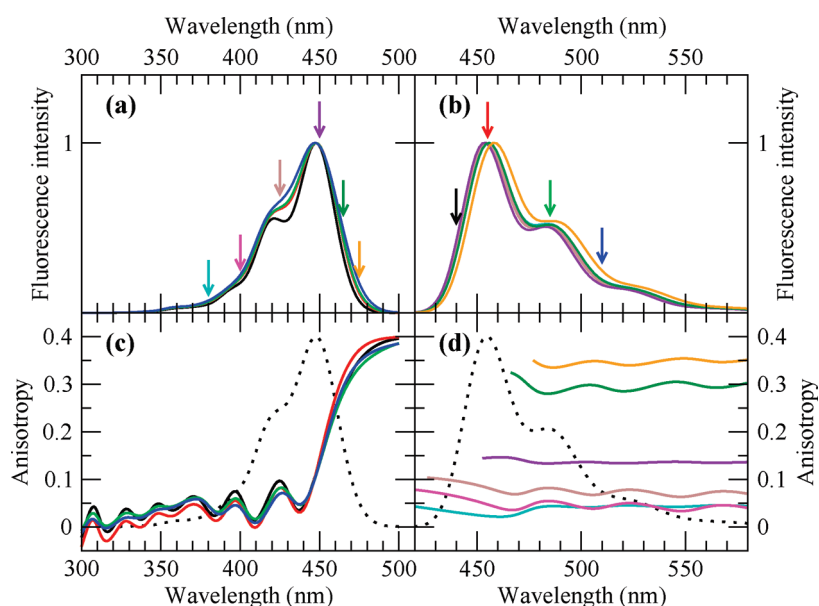


**Figure 4.** Calculated spectra of **O1** in a rigid polar matrix. (a) Calculated fluorescence excitation spectra and (c) fluorescence excitation anisotropy spectra obtained for different emission wavelengths (440, 455, 485, 510 nm, chosen to correspond to spectral positions comparable to the experimental ones), as indicated by the arrows of the corresponding colors in panel b. (b) Calculated fluorescence emission spectra and (d) fluorescence emission anisotropy spectra obtained for different excitation wavelengths (380, 400, 425, 450, 465, 475 nm), as indicated by the arrows of the corresponding colors in panel a. In panels c and d, dashed lines report representative calculated excitation and emission spectra, respectively, as guides to the eyes. Parameters:  $\eta = 1.29$  eV,  $\sqrt{2}t = 0.55$  eV,  $\omega_v = 0.18$  eV,  $\varepsilon_v = 0.16$  eV,  $\varepsilon_{or} = 0.28$  eV,  $\sigma = 0.06$  eV,  $T = 90$  K.

(panel d), with the only exception being a narrow region on the blue side of the emission spectrum, where the experimental spectra show a sharp increase not reproduced by the calculated spectra. Indeed, this portion of the spectrum corresponds to the region of the Stokes shift, namely, the wavelength range between the maximum of the absorption (excitation) and emission spectra. Polar solvation is the only source of Stokes shift in our model: because frozen solvents cannot relax, the calculated Stokes shift vanishes in glassy solutions. The experimental observation of a finite Stokes shift in frozen solvents demonstrates the presence of other slow degrees of freedom that are able to relax after excitation even in the rigid matrix. Such degrees of freedom are most probably associated with internal low-frequency vibrational or conformational modes, not contributing to the Franck–Condon shape because of their low frequencies but able to relax after the molecule has been promoted to the electronic excited state. Apart from the narrow region of the Stokes shift, the calculated anisotropy spectra compare very well with the experimental spectra. The excitation anisotropy spectra show some indication of a vibronic structure: in Figure 3c, anisotropy decreases from the red to the blue side of the absorption (excitation) band, but a shoulder is clearly observed around 425 nm, corresponding to the 0–1 vibronic replica of the excitation spectrum, independently of the detection wavelength. Our calculated excitation anisotropy spectra in Figure 4c reproduce this feature very well, confirming its vibronic origin. Indeed, additional vibronic replicas are predicted in the calculated spectra, but are not recognized in the experimental data because of the experimental noise and, most probably, the presence of several sources of inhomogeneous broadening not taken into account in our calculation.

To confirm our results and their interpretation, we also measured the fluorescence excitation and emission spectra and the corresponding anisotropy spectra of **D1** and **O1** in

supercooled PG at 190 K (available in the Supporting Information, Figures S1 and S2). The spectra are very similar to those obtained in glassy 2-MeTHF: the dependence of the excitation/emission spectra on the emission/excitation wavelength is confirmed; the anisotropy of **D1** has a roughly constant value between 0.35 and 0.4 (see Figure S1, Supporting Information); and the anisotropy of **O1** (Figure S2, Supporting Information) shows an impressive dependence on the excitation wavelength, as already observed in 2-MeTHF. These results confirm that the peculiar behavior of anisotropy spectra of **O1** is not related to a specific solvent, but can be observed when the octupolar compound is dissolved in any polar solvent. To further confirm the generality of our results, we repeated the measurements on another octupolar compound, **O2** (crystal violet), in supercooled PG at 190 K. The experimental data, reported in Figure 5, show a behavior similar to that observed for **O1**.

We calculated fluorescence excitation and emission spectra and corresponding anisotropy spectra of **O2** (which was parametrized in ref 36): the results are reported in Figure 6. These spectra were calculated for a rigid matrix (no relaxation of the solvent distribution prior to fluorescence) at 190 K. Also for **O2**, the agreement of the calculated results with the experimental behavior is very good in terms of the excitation and emission band shapes and the anisotropy spectra.

The ultimate confirmation of the special role played by polar solvation in the optical spectra of octupolar ICT chromophores is obtained by the spectral analysis of **D1** and **O1** in a nonpolar rigid matrix. Specifically, we used undercooled DHN (decalin) at 210 K (**O2** is insoluble in this solvent). The results for **O1** are reported in Figure 7, whereas the results for **D1** can be found in the Supporting Information (Figure S3). Spectra collected in DHN show a distinctively different behavior compared to spectra collected in polar matrixes (either 2-MeTHF or PG). For both **D1** (Figure S3, Supporting Information) and **O1** (Figure 7), the



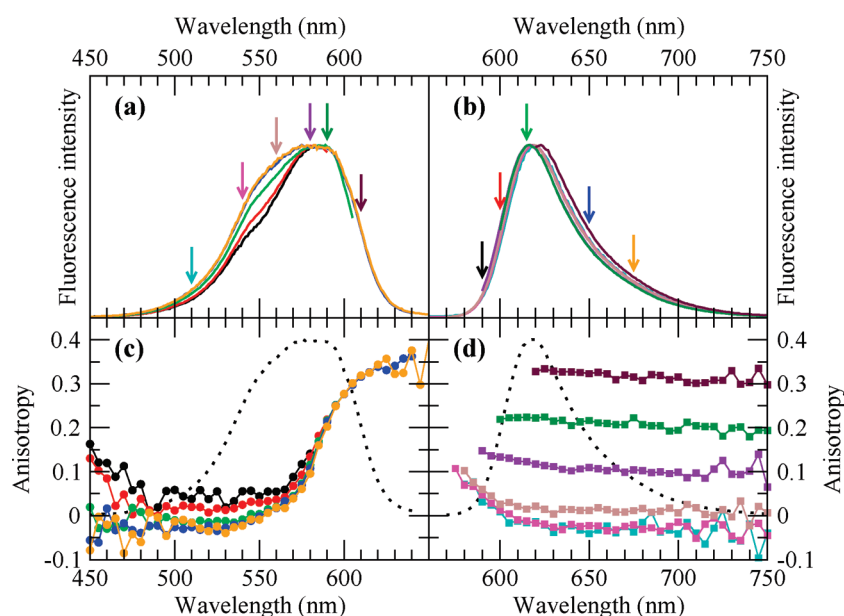


**Figure 5.** Spectra of O2 in glassy PG at 190 K. (a) Fluorescence excitation spectra and (c) fluorescence excitation anisotropy spectra obtained by detecting at different emission wavelengths (590, 600, 615, 650, 675 nm), as indicated by the arrows of the corresponding colors in panel b. (b) Fluorescence emission spectra and (d) fluorescence emission anisotropy spectra obtained by exciting at different wavelengths (510, 540, 560, 580, 590, 610 nm), as indicated by the arrows of the corresponding colors in panel a. In panels c and d, dashed lines report representative excitation and emission spectra, respectively, as guides to the eyes.

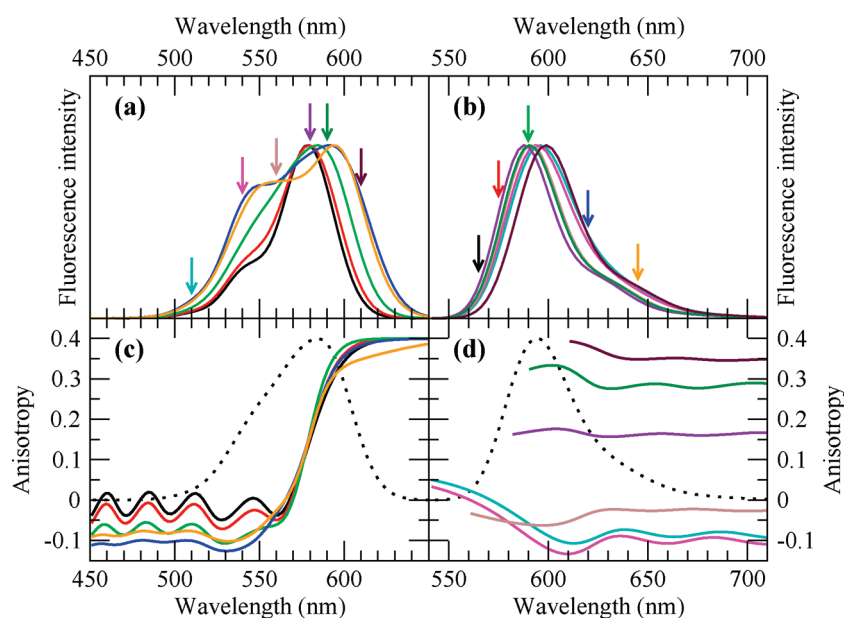


**Figure 6.** Calculated spectra of O2 in a rigid polar matrix. (a) Calculated fluorescence excitation spectra and (c) fluorescence excitation anisotropy spectra obtained for different emission wavelengths (565, 575, 590, 620, 645 nm, chosen to correspond to spectral positions comparable to the experimental ones), as indicated by the arrows of the corresponding colors in panel b. (b) Calculated fluorescence emission spectra and (d) fluorescence emission anisotropy spectra obtained for different excitation wavelengths (510, 540, 560, 580, 590, 610 nm), as indicated by the arrows of the corresponding colors in panel a. In panels c and d, dashed lines report representative calculated excitation and emission spectra, respectively, as guides to the eyes. Parameters:  $\eta = 0.53$  eV,  $\sqrt{2}t = 0.91$  eV,  $\omega_v = 0.13$  eV,  $\epsilon_v = 0.08$  eV,  $\epsilon_{or} = 0.27$  eV,  $\sigma = 0.04$  eV,  $T = 190$  K.

excitation and emission spectra are hardly dependent on the detection or excitation wavelength; only for excitation in the red tail of the absorption spectrum of O1 can one observe an emission spectrum having a very pronounced long-wavelength feature (dark green line), a typical signature of excimers or aggregates (a similar behavior, but much less evident, is observed

for D1). As expected for dipolar chromophores in rigid matrixes, the anisotropy of D1 stays almost constant at values ( $\sim 0.3$ ) not far from the limiting 0.4 value.

The excitation anisotropy spectra of O1 (Figure 7c) are, however, strikingly different from those obtained in polar matrixes: the excitation anisotropy stays quite constant around



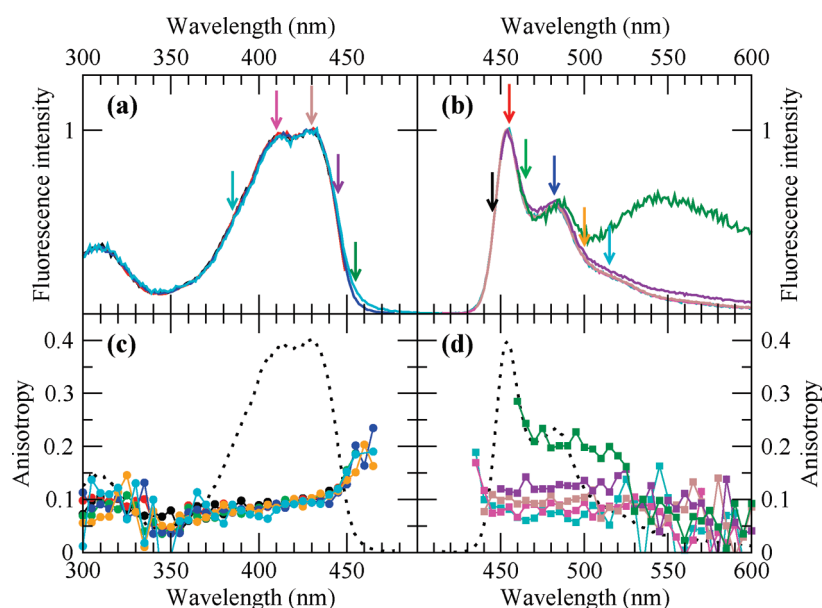


**Figure 7.** Spectra of **O1** in glassy DHN (decalin) at 210 K. (a) Fluorescence excitation spectra and (c) fluorescence excitation anisotropy spectra obtained by detecting at different emission wavelengths (445, 455, 465, 482, 500, 515 nm), as indicated by the arrows of the corresponding colors in panel b. (b) Fluorescence emission spectra and (d) fluorescence emission anisotropy spectra obtained by exciting at different wavelengths (385, 410, 430, 445, 455, nm), as indicated by the arrows of the corresponding colors in panel a. In panels c and d, dashed lines report representative excitation and emission spectra, respectively, as guides to the eyes.

the value of 0.1 throughout the excitation spectrum, with just a weak increase in the far red tail of the excitation band, where experimental evidence suggests that absorption is mainly due to aggregates or corresponding emission stems from excimer species (see the dark green emission spectrum in Figure 7b). Analogously, the emission anisotropy (Figure 7d) stays constant around the value of 0.1 throughout the emission spectrum, independently of the excitation wavelength, with the only exception being excitation in the far red tail of the absorption spectrum, where the anisotropy is higher (dark green symbols). In principle, an increase of the fluorescence anisotropy upon excitation in the red edge of the absorption band in a nonpolar solvent might be due to low-energy conformational modes, the same as that responsible for the finite Stokes shift in the glassy solvent. However, we believe that, in this case, the residual red-edge effect is due to emission from aggregates or excimers. In particular, we calculated fluorescence anisotropy spectra for a small  $\epsilon_{\text{or}}$  value, to simulate the effects of a slightly dipolar solvent or of low-energy conformational modes and found that the calculated excitation anisotropy started to increase in correspondence to the wavelength of maximum absorption (i.e., well blue-shifted with respect to the experimental observation). This further supports our conclusions that the observed increase in fluorescence anisotropy measured for red-edge excitation in nonpolar solvents is related to the presence of aggregates and/or excimers, as suggested by the shape of the corresponding emission spectrum. The calculated spectra of **O1** in a nonpolar matrix ( $\epsilon_{\text{or}} = 0$ ; see Figure S4 in the Supporting Information) predict excitation and emission spectra independent of the emission and excitation lines, respectively, as well as a constant anisotropy of  $r = 0.1$ , in good agreement with the experimental results.

## 5. DISCUSSION AND CONCLUSIONS

The fluorescence and fluorescence anisotropy spectra measured for two octupolar ICT chromophores show some features

that are clearly related to the effects of polar solvation in rigid matrixes. In particular, emission/excitation spectra depend on the excitation/emission wavelength, and anisotropy is strongly dependent on the excitation wavelength.

Similar effects have already been reported in the literature for other chromophores with  $C_3$  symmetry (although for single-wavelength excitation and/or emission).<sup>44,47–49</sup> These phenomena are usually discussed in terms of red-edge effects and/or symmetry-breaking phenomena.<sup>44,47,50</sup> However, these explanations have only a qualitative basis and are somewhat incomplete. Based on our extensive experimental and theoretical work, we are now in the position to clarify some points, in particular, the difference between symmetry breaking in the excited state, the lowering of the molecular symmetry due to polar solvation, and their relation to so-called red-edge effects.

The first excited state of octupolar ICT chromophores is doubly degenerate as long as the nuclear geometry is undistorted, but the degeneracy is removed by any (even tiny) distortion of the molecular geometry along one of the  $E$ -symmetry vibrational coordinates. More specifically, plotting the energy of the two lowest excited states in the plane spanned by the two  $E$ -symmetry vibrational coordinates, one obtains a conical intersection between the two potential energy surfaces (PESs).<sup>35</sup> In particular, the two PESs are degenerate just at the origin (no distortion), but away from the origin, the two PESs split: the lower-energy PES shows three equivalent absolute minima for distortions along the three molecular branches, whereas the higher-energy PES maintains a single minimum at the origin. The presence of three minima in the PES relevant to the first excited state makes this state multistable. Each of the three minima corresponds to a distortion along one molecular branch, and the corresponding electronic distribution is mainly localized on the corresponding branch. This excited-state multistability can correspond or not to symmetry breaking in the excited state: if the electronic excitation travels from one minimum to the

other faster than molecular vibrations, the global symmetry is recovered, whereas if the electronic excitation stays in one single minimum for a time longer than a vibrational period, symmetry is effectively broken, and the electronic excited state is localized over one single branch.<sup>35</sup> What is more interesting for our discussion is that polar solvation favors symmetry breaking in the excited state of octupolar ICT chromophores: because each of the three minima corresponds to a dipolar electronic distribution, the interaction with a polar solvent stabilizes the corresponding dipolar excited state, truly breaking the symmetry along the relevant molecular branch.<sup>35</sup> The three minima are equally stabilized by polar solvation, and the hopping between them is associated with the dynamics of the solvation coordinate (typically on the order of a few picoseconds). However, each of the minima corresponds to a broken-symmetry molecular geometry (nuclei relax faster than the solvation dynamics). This is the reason why octupolar ICT chromophores always undergo symmetry breaking in the excited state when dissolved in polar solvents, as demonstrated by the strongly solvatochromic behavior of their fluorescence spectra.<sup>29,35</sup>

This symmetry-breaking phenomenon (or Jahn–Teller distortion) in the relaxed excited state of octupolar ICT chromophores (dissolved in polar solvents) cannot explain the behavior of fluorescence anisotropy as a function of the excitation wavelength. In fact, as long as the symmetry is preserved in the ground state, the vertical excitation cannot (by definition) break the molecular symmetry, so that the vertical excitation always corresponds to a symmetric ICT involving the three molecular branches. Once this vertical excited state is reached, excitation can localize with the same probability over any of the three molecular branches, so that the expected value of fluorescence anisotropy is invariably 0.1: symmetry breaking in the excited state has no influence on the anisotropy value. To explain the peculiar behavior of fluorescence anisotropy in octupolar ICT chromophores (the sharp deviation from the 0.1 value for excitation in the red edge of the excitation band), it is necessary to invoke some lowering of the symmetry of the molecules in solution *before* their excitation. In that way, the degeneracy between the first two excited states is removed (see right panel of Scheme 2), and the vertical excitation preferentially promotes the system to the lower-energy or higher-energy excited state according to the excitation wavelength. Because the two excited states are polarized along perpendicular directions and because fluorescence always occurs from the lowest-energy excited state, anisotropy will depend on the excitation wavelength, being high (0.4 limit) for excitation in the red edge of the absorption band and low (−0.2 limit) for excitation in the blue edge.

We can now discuss the origin of the lowering of the molecular symmetry. An isolated molecule having a stable ground state has no reason to distort its symmetry. However, one can expect a lowering of the molecular symmetry for highly symmetric molecules dissolved in polar solvents. Highly symmetric molecules, such as octupolar ICT chromophores, have no permanent dipole moment, and one expects a vanishing value for the solvation reaction field at equilibrium. At finite temperature, however, different solvent configurations (orientations) are possible, corresponding to finite values of the reaction field, according to a typical Boltzmann distribution.<sup>35</sup> The solute molecules experiencing a finite reaction field will respond by readjusting their electronic distribution and geometry, giving rise to molecular structures with lower symmetry.<sup>36</sup> Therefore, at any finite temperature, the solution contains a collection of solute molecules experiencing different reaction fields.<sup>35,36</sup> The

spectroscopic response of the ensemble will be given by the sum of the responses of all molecules, leading to the inhomogeneous broadening of optical spectra.

Some of the phenomena that we report here for octupolar ICT chromophores are often referred to as red-edge effects.<sup>40</sup> Red-edge effects were observed and discussed for the first time in the early 1970s, when, in a few different laboratories, it was found that the spectroscopic properties of fluorophores embedded in rigid or highly viscous media do not conform to classical rules. For example, it was found that fluorescence spectra can depend on the excitation wavelength<sup>51,52</sup> and that energy-transfer processes, if any, can fail for excitation in the red edge of the absorption band.<sup>53,54</sup> These red-edge effects were related to inhomogeneous broadening of the spectra, arising from solute–solvent energy distribution. The broadening, in fact, together with the rigid nature of the medium, allows for photoselection by excitation or emission wavelength.<sup>40</sup> Inhomogeneous broadening can explain the dependence of fluorescence excitation/emission spectra on the emission/excitation wavelength, as well as the lack of energy transfer for excitation at the red edge, but it does not justify the behavior of fluorescence anisotropy that we reported for octupolar ICT chromophores. In fact, even for excitation at the red edge of the absorption band (i.e., by photoselection of the chromophores absorbing at the bottom of the transition-energy distribution), an anisotropy value of 0.4 cannot be explained, as the maximum anisotropy for a  $C_3$ -symmetric chromophore is 0.1. An ensemble of undistorted ( $C_3$ -symmetric) chromophores absorbing at different wavelengths because of inhomogeneous broadening cannot have anisotropy values beyond 0.1. Higher anisotropy values can arise only because of symmetry lowering that removes the degeneracy of the two lowest-energy and orthogonally polarized excitations. In other words, one must recognize that inhomogeneous broadening induced by polar solvation is responsible for the presence in solution of molecules with lower symmetry with respect to the highly symmetric structure expected at equilibrium ( $F_{or} = 0$ ), thus determining the peculiar behavior of anisotropy spectra.

The exciton model is often employed in the literature to describe optical spectra of octupolar ICT chromophores.<sup>55</sup> According to this approach, the octupolar molecule is described as being composed of three independent but interacting equivalent chromophores, corresponding to the three molecular branches. Upon excitation with polarized radiation, the branch aligned along the polarized field is preferentially excited. According to the strength of electronic coupling between the three branches, the electronic excitation, initially localized on the excited branch, stays localized (weak coupling) or delocalizes over the three branches (strong coupling). The hopping process is nothing but electronic energy transfer among identical “chromophores” (omotransfer). This hopping or omotransfer process is responsible for depolarization of the emission, each branch being aligned at  $\pm 120^\circ$  with respect to the others, leading again to the 0.1 value for fluorescence anisotropy in  $C_3$ -symmetric “multichromophores”.<sup>44,47</sup> If the three branches are no longer equivalent because of their different interactions with the local environment, each branch will absorb at a different energy. If excitation is in the blue edge of the absorption band, exergonic hopping is allowed toward the branches absorbing at lower energy, so that emission will be depolarized (anisotropy value of 0.1). For excitation at the red edge, the transfer among branches is hindered because it would be endergonic, so that emission will occur from the very same branch that was excited,

leading to the limiting anisotropy value of 0.4.<sup>44,47</sup> The excitonic picture for octupolar ICT chromophores is simple and direct, and it provides an easily accessible qualitative description of anisotropy red-edge effects. However, the exciton model hardly applies to branched molecules such as **O1** or **O2**, in which the three chromophores (i.e., the three molecular branches) are mutually conjugated through the common core, giving rise to a delocalized electron system in two dimensions.<sup>28,36</sup> In this case, essential-state models that properly account for charge transfer are definitely needed. In any case, in the presence of a sizable electronic coupling between the branches, the exciton model itself predicts a totally symmetric ground state for the branched system, namely, two degenerate *E*-symmetry excited states, and another totally symmetric excited state at higher energy.<sup>55,56</sup> For symmetry reasons, the two degenerate excited states are allowed by linear absorption, whereas the higher-energy excited state, being totally symmetric, is a dark state for linear absorption and is a two-photon active state. For sizable coupling between the branches, it is thus not correct to talk about excitations of single branches, because the excitation is (at least partially) delocalized over the three branches.<sup>55,56</sup> Considering three excited states allowed by linear absorption (each one corresponding to the excitation of one branch) is not correct either, because only two of the excited states are allowed by one-photon absorption. Only for completely noninteracting chromophores could three independent excitations be considered, but in this case, the exciton coupling would be zero, and the anisotropy would amount to the constant 0.4 value. Regardless of the description used for octupolar ICT chromophores, either the exciton picture or the essential-state charge-transfer model, the most reliable interpretation of red-edge effects, including the anisotropy behavior, relies on the presence of two orthogonally polarized degenerate excited states, whose degeneracy can be removed by fluctuations of the medium at finite temperature.

Essential-state models have a major advantage over the exciton model for branched ICT chromophores. In fact, by properly accounting for electronic, vibrational, and polar solvation degrees of freedom and for their mutual interactions, essential-state models allow for a detailed calculation of optical spectra. In particular, in this work, we were able to calculate, for the first time, fluorescence emission and excitation anisotropies for dipolar and octupolar chromophores in glassy matrixes of different polarities. The calculated anisotropy spectra quantitatively compare with experimental data, confirming the reliability of the essential-state approach to the optical spectra of ICT chromophores. Moreover, the proposed analysis sheds light on some fundamental questions in molecular spectroscopy, definitively assessing the issue of red-edge effects in highly symmetric molecules.

In conclusion, in this article, we reported the fluorescence excitation and emission spectra and the corresponding anisotropy spectra for an octupolar ICT chromophore and its corresponding dipolar branch. Spectra were recorded at low temperature in glassy solvents of different polarities. In the polar glassy solvents, excitation/emission spectra were found to depend on the emission/excitation wavelength, whereas in the glassy apolar solvent, no dependence was observed. This behavior can be explained as being due to the photoselection of different subsets of molecules from the frozen inhomogeneous distribution arising from the solute–solvent interaction. The most interesting result is related to the anisotropy spectra. For an octupolar chromophore in a glassy polar solvent, the

fluorescence anisotropy changes strongly when the excitation wavelength is varied throughout the absorption band, whereas in an apolar glassy matrix, no marked dependence is observed. Incidentally, we stress here that, to the best of our knowledge, this is the first time that fluorescence anisotropy spectra of octupolar ICT chromophores in a glassy apolar medium have been reported. The results in polar solvents were also confirmed for a second octupolar ICT chromophore, Crystal Violet. A model for the detailed and quantitative interpretation of these results has been proposed, based on an essential-state description of the electronic structure of the chromophores and including electron–phonon coupling and solvation interaction. Our model not only provides a qualitative interpretation of excitation and emission spectra and anisotropy spectra of ICT chromophores, but also allows for a quantitative prediction of these properties. Essential-state models allow for a clear distinction to be made between symmetry-breaking phenomena in the excited state (responsible for fluorescence solvatochromism) and disorder-induced symmetry lowering (responsible for red-edge effects). They provide a valid and more consistent alternative to the standard exciton model, which hardly applies to branched chromophores in which through-bond, coherent interactions are responsible for delocalization phenomena that cannot be described by a simple hopping mechanism between independent chromophoric units.<sup>28</sup> The availability of reliable models for the description of branched ICT chromophores in different media is of great importance for the knowledge-guided development of molecular-based systems with optimized properties for various applications, such as molecular electronics, nonlinear optics, and artificial light harvesting.

## ■ ASSOCIATED CONTENT

**S Supporting Information.** Expressions for the transition energies and dipole moments in the two-state and four-state models, fluorescence excitation and emission spectra and corresponding anisotropy spectra of **D1** and **O1** in glassy propylene glycol (190 K) and of **D1** in undercooled decahydronaphthalene (210 K), and calculated excitation and emission spectra and corresponding anisotropy spectra of **O1** in undercooled decahydronaphthalene (210 K). This material is available free of charge via the Internet at <http://pubs.acs.org>.

## ■ AUTHOR INFORMATION

### Corresponding Author

\*E-mail: francesca.terenziani@unipr.it. Tel.: +39 0521 905453. Fax: +39 0521 905556.

## ■ ACKNOWLEDGMENT

This work was supported by MIUR through PRIN2006-031511 “Chromophores in organic and hybrid nanostructures: supramolecular engineering of photonic properties” and by Fondazione Cariparma through the project 2010.0329 “Fenomeni di trasferimento di carica e di energia in materiali molecolari per applicazioni fotovoltaiche innovative”.

## ■ REFERENCES

- (1) Reichardt, C. *Chem. Rev.* **1994**, *94*, 2319.
- (2) Le Droumaguet, C.; Mongin, O.; Werts, M. H. V.; Blanchard-Desce, M. *Chem. Commun.* **2005**, 2802.



- (3) Reichardt, C. *Pure Appl. Chem.* **2008**, *80*, 1415.
- (4) Signore, G.; Nifos, R.; Albertazzi, L.; Storti, B.; Bizzarri, R. *J. Am. Chem. Soc.* **2010**, *132*, 1276.
- (5) Koch, N. *ChemPhysChem* **2007**, *8*, 1438.
- (6) Shirota, Y.; Kageyama, H. *Chem. Rev.* **2007**, *107*, 953.
- (7) Kanibolotsky, A. L.; Perepichka, I. F.; Skabara, P. J. *Chem. Soc. Rev.* **2010**, *39*, 2695.
- (8) Wenger, O. S. *Acc. Chem. Res.* **2011**, *44*, 25.
- (9) Roquet, S.; Cravino, A.; Leriche, P.; Alévêque, O.; Frère, P.; Roncali, J. *J. Am. Chem. Soc.* **2006**, *128*, 3459.
- (10) Currie, M. J.; Mapel, J. K.; Heidel, T. D.; Goffri, S.; Baldo, M. A. *Science* **2008**, *321*, 226.
- (11) Brédas, J.-L.; Norton, J. E.; Cornil, J.; Coropceanu, V. *Acc. Chem. Res.* **2009**, *42*, 1691.
- (12) Roncali, J. *Acc. Chem. Res.* **2009**, *42*, 1719.
- (13) Nantalaksakul, A.; Mueller, A.; Klaikherd, A.; Bardeen, C. J.; Thayumanavan, S. *J. Am. Chem. Soc.* **2009**, *131*, 2727.
- (14) Delgado, J. L.; Bouit, P.-A.; Filippone, S.; Herranz, M.; Martin, N. *Chem. Commun.* **2010**, *46*, 4853.
- (15) Würthner, F.; Meerholz, K. *Chem.—Eur. J.* **2010**, *16*, 9366.
- (16) Walker, B.; Kim, C.; Nguyen, T.-Q. *Chem. Mater.* **2011**, *23*, 470.
- (17) Strehmel, B.; Strehmel, V. In *Advances in Photochemistry*; Neckers, D. C., Jenks, W. S., Wolff, T., Eds.; John Wiley & Sons: New York, 2005; Vol. 29, p 111.
- (18) Marder, S. R. *Chem. Commun.* **2006**, 131.
- (19) He, G. S.; Tan, L.-S.; Zheng, Q.; Prasad, P. N. *Chem. Rev.* **2008**, *108*, 1245.
- (20) Terenziani, F.; Katan, C.; Badaeva, E.; Tretiak, S.; Blanchard-Desce, M. *Adv. Mater.* **2008**, *20*, 4641.
- (21) Kim, H. M.; Cho, B. R. *Chem. Commun.* **2009**, 153.
- (22) Pawlicki, M.; Collins, H. A.; Denning, R. G.; Anderson, H. L. *Angew. Chem., Int. Ed.* **2009**, *48*, 3244.
- (23) Sullivan, P. A.; Dalton, L. R. *Acc. Chem. Res.* **2010**, *43*, 10.
- (24) Hales, J. M.; Matichak, J.; Barlow, S.; Ohira, S.; Yesudas, K.; Brédas, J.-L.; Perry, J. W.; Marder, S. R. *Science* **2010**, *327*, 1485.
- (25) Balzani, V.; Ceroni, P.; Maestri, M.; Vicinelli, V. *Curr. Opin. Chem. Biol.* **2003**, *7*, 657.
- (26) Wasielewski, M. R. *Acc. Chem. Res.* **2009**, *42*, 1910.
- (27) Wan, Y.; Yan, L.; Zhao, Z.; Ma, X.; Guo, Q.; Jia, M.; Lu, P.; Ramos-Ortiz, G.; Maldonado, J. L.; Rodriguez, M.; Xia, A. *J. Phys. Chem. B* **2010**, *114*, 11737.
- (28) Goodson, T. G., III. *Acc. Chem. Res.* **2005**, *38*, 99.
- (29) Sissa, C.; Parthasarathy, V.; Drouin-Kucma, D.; Werts, M. H. V.; Blanchard-Desce, M.; Terenziani, F. *Phys. Chem. Chem. Phys.* **2010**, *12*, 11715.
- (30) Lakowicz, J. R. *Principles of Fluorescence Spectroscopy*; Kluwer Academic/Plenum Publishers: New York, 1999.
- (31) Painelli, A.; Terenziani, F. *Chem. Phys. Lett.* **1999**, *312*, 211.
- (32) Boldrini, B.; Cavalli, E.; Painelli, A.; Terenziani, F. *J. Phys. Chem. A* **2002**, *106*, 6286.
- (33) Terenziani, F.; Painelli, A.; Katan, C.; Charlot, M.; Blanchard-Desce, M. *J. Am. Chem. Soc.* **2006**, *128*, 15742.
- (34) Terenziani, F.; Przhonska, O. V.; Webster, S.; Padilha, L. A.; Slominsky, Y. L.; Davydenko, I. G.; Gerasov, A. O.; Kovtun, Y. P.; Shandura, M. P.; Kachkovski, A. D.; Hagan, D. J.; Stryland, E. W. V.; Painelli, A. *J. Phys. Chem. Lett.* **2010**, *1*, 1800.
- (35) Terenziani, F.; Sissa, C.; Painelli, A. *J. Phys. Chem. B* **2008**, *112*, 5079.
- (36) Campo, J.; Painelli, A.; Terenziani, F.; Regemorter, T. V.; Beljonne, D.; Goovaerts, E.; Wenseleers, W. *J. Am. Chem. Soc.* **2010**, *132*, 16467.
- (37) Mulliken, R. S. *J. Am. Chem. Soc.* **1952**, *74*, 811.
- (38) Oudar, J. L.; Chemla, D. S. *J. Chem. Phys.* **1977**, *66*, 2664.
- (39) Cho, M. *J. Phys. Chem. A* **1999**, *103*, 4712.
- (40) Demchenko, A. P. *Luminescence* **2002**, *17*, 19.
- (41) Andrews, S. S. *J. Chem. Educ.* **2004**, *81*, 877.
- (42) When calculating spectra in glassy matrixes, the  $\eta$  parameter is slightly renormalized to account for the energy shift of the absorption band, probably because of the change in the refractive index of the solvents in the low-temperature glass phase.
- (43) Hall, R. D.; Valeur, B.; Weber, G. *Chem. Phys. Lett.* **1985**, *116*, 202.
- (44) Verbouwe, W.; Van der Auweraer, M.; De Schryver, F. C.; Piet, J. J.; Warman, J. M. *J. Am. Chem. Soc.* **1998**, *120*, 1319.
- (45) Weber, G. *Biochemistry* **1952**, *51*, 145.
- (46) Greenspan, H.; Fischer, E. *J. Phys. Chem.* **1965**, *69*, 2466.
- (47) Stahl, R.; Lambert, C.; Kaiser, C.; Wortmann, R.; Jakober, R. *Chem.—Eur. J.* **2006**, *12*, 2358.
- (48) Dvorák, M.; Michl, M.; Almonasy, N.; Nepraš, M.; Ladd, N.; Fidler, V. *J. Fluoresc.*, published online May 4, 2010, <http://dx.doi.org/10.1007/s10895-010-0668-3>.
- (49) Jia, M.; Ma, X.; Yan, L.; Wang, H.; Guo, Q.; Wang, X.; Wang, Y.; Zhan, X.; Xia, A. *J. Phys. Chem. A* **2010**, *114*, 7345.
- (50) Bangal, P. R.; Lam, D. M. K.; Peteanu, L. A.; Van der Auweraer, M. *J. Phys. Chem. B* **2004**, *108*, 16834.
- (51) Galley, W. C.; Purkey, R. M. *Proc. Natl. Acad. Sci. U.S.A.* **1970**, *67*, 1116.
- (52) Rubinov, A. N.; Tomin, V. I. *Opt. Spektrosk.* **1970**, *29*, 1082.
- (53) Weber, G. *Biochem. J.* **1960**, *75*, 335.
- (54) Weber, G.; Shinitzky, M. *Proc. Natl. Acad. Sci. U.S.A.* **1970**, *65*, 823.
- (55) Beljonne, D.; Wenseleers, W.; Zojer, E.; Shuai, Z.; Vogel, H.; Pond, S. J. K.; Perry, J. W.; Marder, S. R.; Brédas, J.-L. *Adv. Funct. Mater.* **2002**, *12*, 631.
- (56) Katan, C.; Terenziani, F.; Mongin, O.; Werts, M. H. V.; Porrès, L.; Pons, T.; Mertz, J.; Tretiak, S.; Blanchard-Desce, M. *J. Phys. Chem. A* **2005**, *109*, 3024.